

Cite this: DOI: 00.0000/xxxxxxxxxx

Predicting Elemental Boiling Points from First Principles[†]Jan-Michael Mewes^{*a,b}

Received Date

Accepted Date

DOI: 00.0000/xxxxxxxxxx

The normal boiling point (NBP) is a fundamental property of liquids and marks the intersection of the Gibb's free energies of the liquid and the gas phase at ambient pressure. In this work, we present the first comprehensive demonstration of an approach to calculate the boiling point of atomic liquids from first-principles molecular-dynamics simulations. To this end, we combine thermodynamic integration (TDI) and perturbation theory (TPT) with a density-functional theory (DFT) Hamiltonian to deliver converged absolute liquid free energies and entropies. Linear extrapolation to the intersection with the gas phase provides NBPs, which are corrected for systematic over- or under-binding of the DFT Hamiltonian, thereby eliminating any strong dependency on the density functional. Through fine-tuning of the TDI, we reduced the walltime from weeks to about a day per element (10–20k core-hours), which enables extensive testing for B, Al, Na, K, Ca, Sr, Ba, Mn, Cu, Xe and Hg. This demonstrates the excellent performance and particular robustness of the approach. With a mean absolute deviation (MAD) of less than 2% from experimental references, and very similar accuracy for liquid entropies (MAD 2.3 J/(mol*K), 2% relative), the overall deviation is several times smaller than the variation between literature values for several elements.

1 Introduction

The computational prediction and study of phase transitions is an active field of research.¹ The lion's share of this research focuses on transitions between condensed phases like melting or solid-solid transitions,^{2–7} as these are most relevant for real-world applications as, *e.g.*, two polymorphs of the same substance can have significantly different properties. Perhaps because of this general focus, the prediction of NBPs from first-principle simulations is a sparsely populated field of research. The only other published study known to the author that demonstrates a calculation of NBPs largely based on a first-principles methodology is by Nakai and coworkers.⁸ For this, they introduce the so-called harmonic solvation model (HSM) for calculating liquid free energies with a polarizable-continuum model (PCM). The HSM differs from the standard approach for thermochemical contributions in the treatment of translational and rotational degrees of freedom. In the HSM, they are replaced with additional vibrational modes resulting from freezing the PCM cavity in the frequency calculations. Comparing liquid free energies obtained with the HSM based on high-level CCSD(T) energies and an MP2 Hessian to free energies of the gas phase obtained with the standard ideal-gas

model, they obtain very reasonable normal boiling points (NBPs) of 109.7°C and 66.9°C for water and ethanol, respectively. However, although the molecules themselves are described with a first-principles methodology, the description of intermolecular interactions in this approach is entirely based on a PCM with highly parametrized non-electrostatic contributions (SMD).⁹ Most other approaches for the prediction of NBPs are entirely empirical data-driven methods that rely on machine-learning and quantitative structure-property relationships (QSPR).^{10–12} As such, they can often be related to the group-contributions method of Joback and Reid.¹³ Although some of these protocols make use of first-principles calculations to refine the predictions,¹¹ there have been no attempts based solely on first-principles methods.

In general, the calculation of phase-transition temperatures through computer simulations can be carried out in two ways: (i) So-called direct approaches attempt to simulate the phase transition either in time (*e.g.* void method or cluster melting),^{14,15} or in space (*e.g.* interface pinning).⁷ Such direct approaches are complicated by super-heating and super-cooling. As a result, all the methods mentioned above are attempts to avoid, mitigate, or minimize these phenomena. (ii) So-called indirect approaches circumvent these problems through calculating Gibbs free energies of the respective phases separately, and subsequently, locate the point of intersection, *i.e.* where $\Delta G = 0$. This not only eliminates the problems with super-heating and cooling, but allows to exploit these phenomena to achieve faster equilibration, *e.g.*, in solid simulations well above the melting point,¹⁶ or here in liquid simulations above the boiling point. Free-energy based ap-

^a Mulliken Center for Theoretical Chemistry, University of Bonn, Beringstr. 4, 53115 Bonn, Germany, janmewes@janmewes.de

^b Centre for Theoretical Chemistry and Physics, The New Zealand Institute for Advanced Study, Massey University Auckland, 0632 Auckland, New Zealand

[†] Electronic Supplementary Information (ESI) available: [details of any supplementary information available should be included here]. See DOI: 00.0000/00000000.

proaches may be further divided into two groups: On the one hand, there are approaches based on relative free energies (iia) (e.g. the pseudo-supercritical path method)¹⁷, and on the other, there are approaches which attempt the calculation of absolute free energies (iib). For a more detailed overview and discussion of these approaches, the interested reader is referred to refs. 18 and 6. Specifically concerning boiling points, direct approaches (i) as well as those focusing on free-energy differences (iia) are problematic due to the drastic differences between the condensed and gaseous phases in terms of volume. Hence, we approach the problem by calculating absolute free energies.

One approach for the calculation of absolute free energies of liquids was recently presented by Kresse and coworkers,¹⁹ and employed to study the melting of silicon and magnesia (MgO).^{19,20} We have further developed this approach to include spin-orbit relativistic effects to explore the physicochemical properties and aggregation state of the super-heavy element Cn.¹⁶ Since Cn has been inferred to be highly volatile,²¹ it was necessary to include the NBP. For this purpose, the herein presented concept was developed. This work describes the adaptation of this approach to efficiently calculate NBPs, as well as the comprehensive testing for a representative set of elements, including insulators, semiconductors, and metals.

An important part of the approach is a linear scaling of the calculated transition temperatures based on the ratio between the cohesive energy calculated at the same level as the free energy, and a high-level reference, *i.e.*, $\lambda = E_{\text{coh}}^{\text{ref}}/E_{\text{coh}}^{\text{DFT}}$. This so-called λ -scaling increases the accuracy and robustness of the approach, in particular concerning the choice of the density-functional approximation (DFA). While the article introducing this correction makes use of a high-level theoretical CCSD(T) reference,¹⁶ this work mostly employs experimental references since such high-level calculations are not readily available for all elements considered here. Although this introduces a certain degree of empiricism, we argue that very similar results would be obtained by using high-level theoretical values, as is demonstrated for Xe.

Before we move to the main article, it bears pointing out that to our surprise, we found the literature to be peppered with conflicting values for the NBPs of common elements, *e.g.*, K (1.5% variation), B (8.7% variation) and Ba (17% variation). This and related uncertainties have been studied in detail by Zhang and coworkers,²² who employed neural networks to rectify conflicts between several major reference books.^{23–27} Exploiting, *e.g.*, the relation between the enthalpy of evaporation and the NBP, they eventually suggested the most probable and consistent values. We will follow their suggestions in this work, which are consistent with our calculations in all but one example. In addition to the sources considered by Zhang and coworkers, we also include values from the prominent Hollemann-Wiberg.²⁸

2 Approach

The normal boiling point (NBP) is defined as the intersection of the Gibbs free energies

$$G(T, p) = U(T) + pV - TS(T) \quad (1)$$

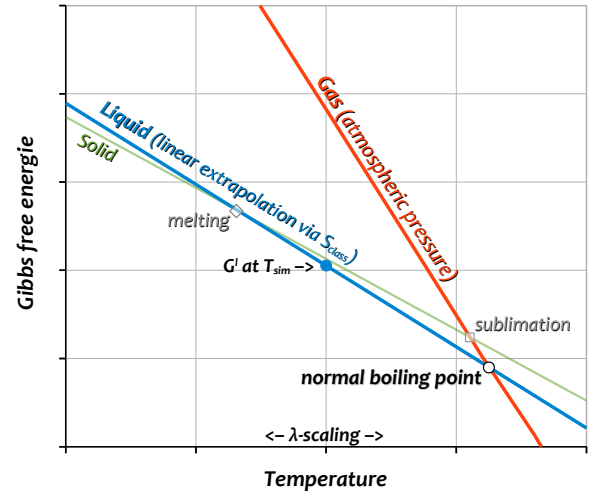


Fig. 1 Plot of the Gibbs free energy of the solid, liquid and gas phases as a function of the temperature to illustrate the employed approach.

of the liquid and gas phase at their respective equilibrium volume at normal pressure (1013 mBar). To locate this point, we calculate the absolute free energy of the liquid G^l at its equilibrium volume ($pV = 0$) in the classical limit using the Born-Oppenheimer approximation at a given simulation temperature T_{sim} through thermodynamic integration (TDI). We integrate from the analytically known non-interacting reference (with the internal energy U_0 and G_0 from eq. (7) in the SI[†]) to the interacting liquid (with U_1 and G_1), which are coupled by the interaction strength λ

$$G_1 = G_0 + \Delta G_{0-1} = G_0 + \int_0^1 d\lambda \langle U_1(\mathbf{R}) - U_0(\mathbf{R}) \rangle_\lambda. \quad (2)$$

TDI is followed by several steps of thermodynamic perturbation theory (TPT) as detailed in the SI[†] to achieve high numerical precision in terms of plane-wave cut-offs and k -point convergence, as well as to include spin-orbit coupling. Adding these contributions to G_1 provides the final G^l .

The integral in eq. (2) is evaluated numerically with an n point Gauss-Lobatto rule, for which it has to be transformed as detailed in the SI[†] to adapt the limits of the integral. This transformation is also used to change the placement of quadrature points by introducing $\kappa = [0..1]$. While a detailed explanation is provided in the SI,[†] the important aspect is that κ and n govern the balance between accuracy and computation effort. The higher κ and n , the more simulations have to be conducted with very small forces, which – depending to some extent on the system – becomes tedious at $\lambda < 0.01$ and strongly increases the demands in human and computer time. A central task of this work is thus to find values for κ and n that are sufficiently accurate yet efficient. All liquid simulations employ 64-atom configurations (Xe: 61) since previous studies have shown this number to provide converged free energies compared to larger cells with > 200 atoms.^{16,19,20}

Having calculated G^l at T_{sim} , the temperature-dependence due to the liquid entropy is approximated linearly, *i.e.*, $S^l = (U^l - G^l)/T_{\text{sim}}$, where U^l is the average of kinetic and potential energy from a canonical MD simulation ($\lambda = 1$). This allows extrapola-

tion to the intersection with the free energy of the non-interacting gas phase G^s as illustrated in Fig. 1. G^s is calculated analytically using eq. (7) in the SI.[†] In addition to linear extrapolation of G^l , we also test an interpolation between up to three values calculated at different temperatures.

Finally, the resulting NBP is corrected for any systematic deviation between the DFA and a high-level theoretical or experimental reference using λ -scaling. To rationalize the λ -scaling, it is instructive to consider that it was initially conceived as an adaptation of upper limit of the integral over the interaction-strength λ in eq. (2) to match the high-level reference. Only later, it was recognized and proven numerically as well as analytically that for a classical system in the Born-Oppenheimer approximation, λ -scaling is equivalent to simply scaling the (transition) temperature,¹⁶ which is much simpler to implement. Following the same logic, λ -scaling can be used to correct the temperature of any (DFT-)MD simulation, or in other words, match the ratio between available kinetic energy and the depth of the potential energy wells to that of the reference. At the corrected temperature, the accessible configuration space of the DFT Hamiltonian is more similar to that of the reference Hamiltonian at the original temperature, such that properties like densities and (classical) entropies are improved systematically.

For the metallic liquids considered here, an additional complication arises through the electronic entropy S_{el} , which is significant at elevated temperature of the NBP (up to 10% of the total S , cf. Tab. 5 in SI)[†], but is not included in the classical S . To address this consistently, we include S_{el} in the internal energy through Fermi-smearing of the orbital populations,²⁹ which corresponds to neglecting the non-classical temperature dependence of G . Exploratory calculations have shown that this only leads to small changes of a few K in the calculated NBPs and is thus acceptable. However, when comparing the calculated liquid entropies to experimental references, including S_{el} in S distinctly improves the agreement (cf. Fig. 3).

3 Results and Discussion

3.1 Detailed Considerations for Xe, K and B

We begin the discussion with a detailed look at Xe, K, and B to establish the capabilities and limitations of the approach for a small but diverse group of elements. In contrast to all other systems considered here, Xe atoms are weakly interacting, and their bulk forms an insulator, like most noble-gas solids.³⁰ As a result of their weakly interacting nature, noble-gas liquids are often considered as prototypical Lenard-Jones fluids. Although this suggests that an atom-pairwise potential may be suitable, it has recently been shown that the melting point of Xe deviates from the experiment by as much as 20 K if three-body effects are omitted.³¹ We employ the PBE and revPBE density-functional approximations (DFAs),^{32–34} both of which are combined with Grimme’s atom-pairwise D3 correction with the default Becke-Johnson damping (in the following just D3).^{35,36} Hence, three-body effects are only taken into account in the DFT part of the calculation. Nevertheless, PBE-D3 accurately recovers the experimental cohesive energy of -0.164 eV of solid *fcc* Xe. Accordingly,

the scaling factor $\lambda = E^{\text{exp}}/E^{\text{calc}}$ is unity. In contrast, revPBE-D3 over-binds slightly with -0.191 eV, resulting in a λ of 0.859.

We calculated free energies of liquid Xe at the experimental NBP of 165 K with both DFAs. With PBE-D3, we moreover explore the parameters for the integration, as well as increasing the simulation temperature T_{sim} to 200 K. The results of these calculations are compiled in Tab. 2, while a breakdown of the liquid free energy is provided in Tab. 1. Inspection shows that all calculations for Xe are in excellent agreement with the experimental NBP of 165 K. The results are moreover virtually identical for both simulation temperatures, and there is excellent agreement between the entropy-based linear extrapolation at each T_{sim} with a direct interpolation between the free energies calculated at 165 K and 200 K. The over-binding of revPBE-D3 evident from $\lambda < 1$ causes the liquid to be too stable and, in turn, the calculated NBP to be too high by 30 K. However, this systematic deviation is quantitatively compensated by λ -scaling. To eliminate the empiricism introduced by this scaling, the experimental cohesive energy in the calculation of λ can be replaced with a high-level theoretical value of -0.166 eV, which has been derived from coupled-cluster calculations and includes zero-point vibrational energies (ZPVE).³⁷ This results in a slight change of the λ s to 1.017 (PBE-D3) and 0.874 (revPBE-D3), and, accordingly, also the calculated NBPs are very similar ranging from 169.2 – 170.5 K.

This brings us to another aspect, namely the influence of ZPVE,

Table 1 Breakdown of the contributions to the free energy for the liquids of Xe, K, and B from TDI and TPT. Following the element, the employed density-functional approximation (DFA), simulation temperature T_{sim} and density ρ are given. The column ΔG provides the contribution of each step, while "total G " is the running sum. "TPT A//B" indicates that TPT was used to correct the free-energy obtained from TDI with method B to that of method A. Θ is the electronic degeneracy of the atoms in the gas phase. The last row provides the free energy of the gas phase at the simulation temperature. All values are given in eV/atom.

step, cut-off, k -grid	ΔG	total G	U	TS
Xenon , PBE-D3, 165 K, $\rho = 2.73$ g/ccm				
non-interacting liquid		-0.1657	0.0213	0.1870
TDI, 150, Γ	-0.0775	-0.2432	-0.1470	0.0962
TPT, 300, Γ	0.0065	-0.2367	-0.1405	0.0962
TPT, 300, 2^3	-0.0001	-0.2368	-0.1406	0.0962
gas phase, $\Theta = 1$		-0.2334	0.0213	0.2547
Potassium , PBEsol, 1000 K, $\rho = 0.696$ g/ccm				
non-interacting liquid		-1.1004	0.1293	1.2297
TDI, 250, Γ	-0.6329	-1.7332	-0.6392	1.1128
TPT, 500, Γ	-0.0003	-1.7335	-0.6397	1.1128
TPT, 500, 2^3	0.0024	-1.7311	-0.6371	1.1128
gas phase, $\Theta = 2$		-1.7076	0.1293	1.8369
Boron , PBE-D3, 4000 K, $\rho = 2.04$ g/ccm				
non-interacting liquid		-3.6408	0.5170	4.1578
TDI, 350, 2^3	-4.8894	-8.5302	-4.8288	3.7015
TPT, 600, 2^3	-0.0072	-8.5375	-4.8360	3.7015
TPT, 600, 3^3	0.0009	-8.5365	-4.8350	3.7015
TPT, PBE//PBE-D3	0.1799	-8.3567	-4.6552	3.7015
TPT, SCAN//PBE-D3	0.2689	-8.2676	-4.5662	3.7015
gas phase, $\Theta = 6$		-7.7326	0.5170	8.2496

which is relatively large for Xe due to its small cohesive energy. Using the ZPVE-uncorrected high-level value from ref. 37 of 0.172 eV (or back-correcting the experimental value) distinctly increases the λ s to 1.053 (PBE-D3) and 0.905 (revPBE-D3), and significantly worsens the agreement with the experiment as evident from the NBPs of 175.5-176 K. This suggests that implicitly including ZPVE *via* the cohesive energy corrects for the absence of ZPE in our otherwise entirely classical approach. Thus, we will use ZPVE-uncorrected λ s in the following. In any case, the relative size of the ZPVE is distinctly smaller in all further examples (cf. Tab. III in ref. 38).

Potassium is a metallic liquid with a NBP of 1047 K²³⁻²⁵ as suggested by Zhang and coworkers,²² while other sources give values of 1026 K,²⁸ 1032 K,^{26,27} and 1040 K.³⁹ Although gaseous K atoms exhibit a strong pairwise interaction in the form of a covalent bond of 0.55 eV, the resulting virial correction (eq. (9) in SI with $\sigma = 3.496 \text{ \AA}$ and $\varepsilon = 0.55 \text{ eV}$)[†] merely amounts to 1.2 meV/atom at 1000 K, and thus hardly affects the NBP ($\Delta T \approx 1 \text{ K}$). Another result of this strong interaction is that potassium vapor is known to consist of about 5% dimers at the NBP.^{39,40} However, exploring the impact of dimerization using the Quantum-Cluster Equilibrium (QCE) approach as implemented in the Peacemaker program^{41,42} revealed that this has negligible influence on the free energy at 1000 K ($< 1 \text{ meV}$). The reason is that the decrease in entropy just cancels the stabilizing effects on internal energy and volume (pV). For reference, the electronic double-degeneracy ($\Theta = 2$) of K atoms stabilizes the gas by about 60 meV, decreasing the BP by about 75 K.

Solid K crystallizes in a body-centred cubic (*bcc*) lattice, for which PBEsol provides excellent agreement with the experimental cohesive energy ($\lambda = 1.002$). We will thus use PBEsol in most calculations, and conduct additional tests with PBE and the dispersion-corrected PBE-D3. To test the consistency of the extrapolation scheme for this metallic system, we conducted free-energy calculations for liquid K at temperatures of 923 K (650°C), 1000 K, 1023 K (750°C) and 1123 K (850°C). For the calculations at 1023 K, we tested three different values for κ (0.75, 0.70 and 0.60). Finally, to establish the sensitivity concerning the employed volume, we conducted additional calculations at 1023 K with the cell-dimensions varied by $\pm 2\%$, corresponding to $\Delta V \approx 6\%$ and $\langle p \rangle = 0.8/-0.5 \text{ kBar}$.

The results for K are compiled in Tab. 2, while a detailed breakdown of the contributions to the free energy for the PBEsol calculation at 1000 K is provided in Tab. 1. Inspection shows that first and foremost, all results obtained with PBEsol are consistent and virtually independent of the tested parameters. Interpolation between the free energies calculated with PBEsol at 923 K, 1023 K, and 1123 K provides virtually the same NBP as the entropy-based extrapolation. The calculations at different volumes afford such consistent NBPs that it is questionable if the differences are significant considering the statistical uncertainties of 1-2 K. Also, the parameters for the numerical integration do not exert any significant influence in the calculated NBP, showing that a value of 0.6 is sufficient. Considering only the results of PBEsol suggests that the NBP of K is 1032 K, in agreement with the CRC Handbook and the Tab. of Physical and Chemical Constants (better known

Table 2 Calculated and experimental normal boiling points (NBPs) of Xe, K and B. Experimental data taken from Holleman-Wiberg as well as from Zhang and coworkers with their suggestions set in bold.^{22,28} Calculated data is given for various functionals (DFAs), simulation temperatures T_{sim} , integration parameters (κ and n), pressures, as well as with and without λ -scaling. "A//B" indicates that TPT was used to calculate the free energy with method A for configurations obtained with method B. The reference cohesive energy used to determine λ is given in eV/atom after the name of the respective element.⁴³ For Xe and K, we also provide NBPs obtained by interpolation between the calculations at 165 K and 200 K (Xe), and 923 K, 1023 K, and 1123 K (K).

DFA, T_{sim} , n , κ	$\lambda (E_{\text{coh}}^{\text{DFT}})$	NBP /K	
		direct	λ -scaled
Xenon , $E_{\text{coh}}^{\text{exp}} = -0.164$		lit. 165.2 K	
PBE-D3, 165, 7, 0.75	1.000	166.9	167.0
PBE-D3, 200, 7, 0.75	1.000	166.5	166.5
PBE-D3, <i>interpolated</i> ,	1.000	166.6	166.7
revPBE-D3, 165, 8, 0.60	0.859	195.2	167.7
Potassium , $E_{\text{coh}}^{\text{exp}} = -0.934$		lit. 1026, 1032, 1047 K	
PBEsol, 1023, 7, 0.60	1.002	1028	1030
PBEsol, 1023, 7, 0.70	1.002	1027	1029
PBEsol, 1023, 7, 0.75	1.002	1028	1030
PBEsol, 923, 7, 0.75	1.002	1027	1029
PBEsol, 1123, 7, 0.75	1.002	1029	1031
PBEsol, <i>interpolated</i>	1.002	1030	1032
PBEsol, 1023, +0.8 kBar	1.002	1027	1028
PBEsol, 1023, -0.5 kBar	1.002	1028	1030
PBE, 1000, 7, 0.60	1.073	968.5	1039
PBE-D3, 1000, 7, 0.60	0.945	1064	1006
PBEsol, 1000, 7, 0.60	1.002	1029	1030
PBEsol//PBE-D3, 1000	1.002	1026	1028
Boron , $E_{\text{coh}}^{\text{exp}} = -5.920$		lit. 3931, 4203 , 4273 K	
PBE-D3, 4000, 6, 0.60	0.916	4643	4252
PBE-D3, 4000, 8, 0.60	0.916	4646	4255
PBE-D3, 4000, 10, 0.60	0.916	4649	4258
PBE//PBE-D3, 4000	0.928	4505	4179
SCAN//PBE-D3, 4000	0.932	4433	4132

as "Kaye and Laby"),^{26,27} whereas the value of 1047 K suggested by Zhang and coworkers (without any discussion of data to support it) appears too high at first glance. However, the deviation of the two values is only about 1.5%, and the results of our calculations vary slightly between the different DFAs.

Compared to PBEsol, PBE-D3 slightly over-binds solid K as evident from $\lambda = 0.945$, whereas plain PBE slightly under-binds, leading to a λ of 1.073. The results for the NBP before λ -scaling are as one would expect: The over-binding PBE-D3 stabilizes the liquid over the gas phase, moving the calculated NBP to higher temperatures (1064 K), while the under-binding PBE provides a lower NBP of 969 K. Interestingly, λ -scaling not only reduces the overall differences but also inverts the sign of the deviation. The scaled NBP of PBE-D3 lies significantly below the PBEsol result at 1006 K, whereas the scaled NBP of PBE lies (just) above it at 1039 K. This over-compensation is presumably a result of using the cohesive energy of the solid at 0 K as the basis for λ -scaling, whereas the NBP is depends on the stability of the liquid. Since differences between the DFAs are certainly more pronounced in

the highly ordered solid than in the disordered liquid, it is to be expected that the correction slightly over-shoots. The notably larger deviation in the scaled NBP of PBE-D3 could moreover be related to certain shortcomings of the D3 correction for densely packed alkaline metals, and it would be interesting to explore how the improved D4 scheme performs here.⁴⁴ Finally, to demonstrate TPT between DFAs, we recalculate 10 configurations from the PBE-D3 simulation with PBEsol. The resulting correction of G^l of 33.3 meV moves the NBP to 1028 K, and thus very close to the consistent PBEsol result.

Bulk boron is a covalently bound semiconductor. The literature values of its NBP vary from 3931 K^{25,28} over 4203 K^{23,24} to 4273 K.^{26,27} The gas phase consists of isolated boron atoms with $\Theta = 6$. To determine the scaling factor λ , we employ α -rhombohedral boron (12 atoms/unit cell) instead of the thermodynamically most stable β -rhombohedral phase (105-108 atoms/unit-cell)⁴⁵ to avoid dealing with partial occupations. Since the energy difference between the two phases is very small,⁴⁵ this should not lead to any significant differences. For α -boron, PBE, PBE-D3 and SCAN provide good agreement with the experimental cohesive energy as evident from the respective λ s of 0.928, 0.919 and 0.932. We calculate the free energy at 4000 K with PBE-D3 and subsequently use TPT to include also SCAN and plain PBE. The calculated NBPs range from 4132 K (SCAN//PBE-D3) over 4179 K (PBE//PBE-D3) to 4258 K (PBE-D3). As such, they are in good agreement ($< 2\%$) with the experimental value of 4203 K suggested by Zhang and coworkers,²² as well as with the value of 4273 K from refs. 26 and 27. In contrast, the value of 3931 K reported in refs. 25 and 28 is too low by $> 5\%$, *i.e.*, more than two times the overall MAD.

To elucidate the influence of the number of quadrature points on the accuracy of the NBP, we conducted the numerical integration for B with 6, 8, and 10 points. Since increasing the number of points includes calculations for increasingly small λ values of 0.0047 (6 points), 0.0010 (8 points) and 0.0003 (10 points), this improves the sampling of the at 4000 K particularly important repulsive part of the configuration space (*cf.* Fig. 4 in SI)[†]. However, there is only small decrease of the value of the integral by ≈ 3 meV/atom from 6 to 8 points, and again by the same amount from 8 to 10 points. Although these deviations are an order of magnitude larger than the statistical error, they translate to a total ΔT of merely 6 K (6 to 10 points), or 0.1% of the NBP.

To summarize, the two most relevant results from this detailed look at Xe, K and B are (i) the approach is robust concerning simulation temperature, the volume, and also the choice of the DFA, and (ii) TDI conducted with 6-8 quadrature points and $\kappa = 0.60$ is sufficiently accurate for the determination of NBPs. This last point is of particular practical relevance since these settings lead to much more stable and efficient simulations compared to the previously used settings. This allowed us to test the approach for many more elements, which we will discuss in the following.

3.2 Additional Elements

We conducted additional calculations for sodium (Na), aluminum (Al), calcium (Ca), strontium (Sr), barium (Ba), manganese

(Mn), and copper (Cu), and mercury (Hg). Their gas phases consist of isolated atoms with $\Theta = 1$ (Ca, Sr, Ba, Hg), 2 (Na, Cu) or 6 (B, Al, Mn). Cu and Ba moreover exhibit low-lying electronically excited states which are significantly populated near their NBPs. This causes a stabilization of the gas phase by 23 meV/atom for Cu and 32 meV/atom for Ba at the NBP (energy differences relative to ref. 39), which in turn significantly affects the calculated NBP. We take this into account pragmatically, *i.e.*, by using fractional degeneracies of 2.19 and 1.18 for Cu and Ba, which quantitatively restores the agreement with the reference values at and around the NBP. A notable interaction between the atoms in the gas phase exists only in case of Na ($\epsilon = 0.75$ eV, $\sigma = 2.76$ Å),⁴⁶ Al ($\epsilon = 1.66$ eV, $\sigma = 2.41$ Å),⁴⁷ and Cu ($\epsilon = 2.03$ eV, $\sigma = 1.98$ Å).⁴⁸ However, similar to K, neither of these experience a significant contribution from the two-body term at the NBP (Na -0.79 meV, Al -0.49 meV, Cu -0.37 meV). The gas phases of Na and perhaps also that of Al and Cu contain some dimers, but as already discussed for K, their influence on the free energy is negligible at the NBP.

For Na, Al, Ca, Sr, Cu, and Hg, the variation between the experimental references is small, and the agreement with the calculated NBPs very good, as evident from Fig. 2 and Tab. 3. The mean absolute deviation (MAD) over all elements with respect to the literature values suggested by Zhang and coworkers is just 1.38% and the mean deviation (MD) -0.25% (this value uses the PBE-D3 results for the alkaline-earth metals, PBE for Mn and PBEsol for K and Na). The results further demonstrate how λ -scaling improves the predicted NBP, in particular, if there exists significant over- or under-binding at the DFT level, *i.e.*, when λ deviates from unity (*cf.* B, Ca/PBEsol, Sr, Hg). As a result, the final λ -scaled NBPs calculated with various DFAs are consistent despite substantial differences in the DFA description of the respective bulk solids (*cf.* PBE/PBE-D3/PBEsol for the alkaline-earth metals). For Na, we included a free energy calculated at a simulation temperature of just 400 K, *i.e.*, just above the melting point as a hardship case for the entropy-based extrapolation. Despite the large ΔT , the resulting NBP is very reasonable at 1000 K.

Mn and Ba stand out from the other results. For Mn, the variation in the experimental NBP is not too large with a range of 2235 – 2373 K (6%),²² whereas the variation between the calculated NBPs is unusually large. We first employed RPBE and subsequently also SCAN because they provide a much better agreement for the cohesive energy of α -Mn (distorted *bcc* with 51 atoms/cell) than PBE, as evident from the respective λ s of 0.916 (RPBE), 0.980 (SCAN), and 0.751 (PBE). This strong over-binding is particularly surprising since PBE tends to under-binding for all other elements considered here and in general.³⁸ However, despite their good agreement for the cohesive energy, the NBPs calculated with RPBE and, in particular, with SCAN fall significantly short of the range of experimental values with relative deviations of 5% and 9% (with respect to the lower value of 2235 K), *i.e.*, several times the MAD. Surprisingly, the calculation with PBE (conducted at an increased temperature of 3200 K to compensate for the strong over-binding) provides an NBP of 2197 K with a relative deviation of just 2%. Although further calculations would be required to draw any ultimate conclusions,

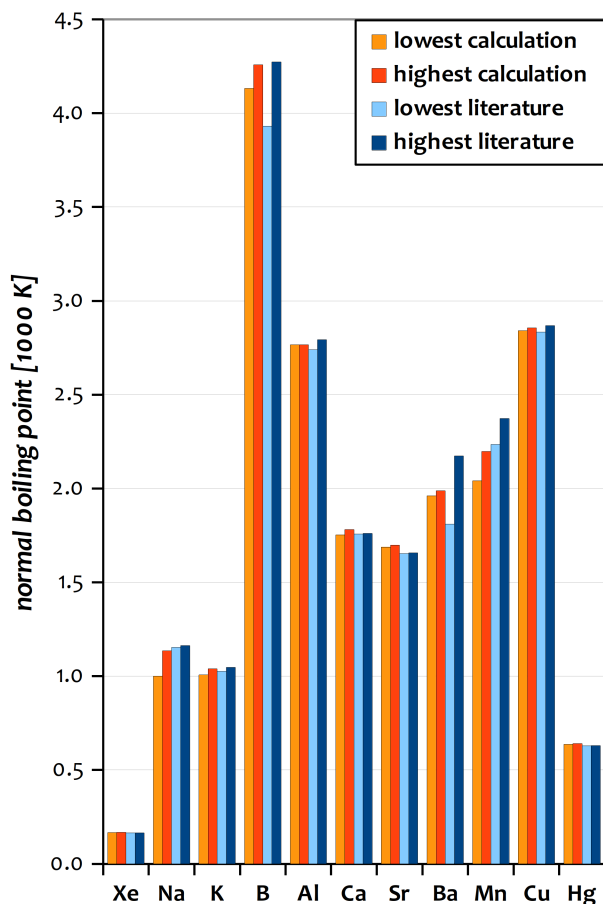


Fig. 2 Plot of the range of calculated values (orange and red, all λ -scaled) against the range of literature values (light and dark blue) as shown in Tabs. 2 and 3. The MAD over all elements with respect to the literature values suggested by Zhang and coworkers is just 1.38% and the MD -0.25% (based on the PBE-D3 results for the alkaline-earth metals, PBE for Mn and PBEsol for K and Na).

these results suggest the good agreement of RPBE and SCAN for the cohesive energy is the result of a fortuitous error compensation between the energy of the bulk and the energy of the isolated atom. Despite its stark over-binding of the solid, PBE appears to provide a consistent description of the solid and liquid, such that λ -scaling based on the cohesive energy of the solid does provide a reasonable NBP. We speculate that these issues are the result of the challenging electronic structure of this *d*-block element with several partially occupied shells. This may impact the calculation of the isolated atom as well as the bulk material and is evident already from the surprisingly strong over-binding of PBE. While it would certainly be interesting to see how an inclusion of non-local exchange and electron-correlation *via* TPT would change the picture, such a focused investigation of a single element is beyond the scope of this general work.

For Ba, the NBPs provided in the literature show a large variation of almost 17%. While the CRC Handbook, as well as the Tables for Physical and Chemical Constants, provide values of 2118–2173 K,^{26,27} other sources provide a distinctly lower value of 1910–1950 K,^{23–25} or even 1810 K in Holleman-Wiberg.²⁸ Zhang and coworkers suggested the value of 1910 K based on a

Table 3 Calculated and experimental NBPs for the second set of elements. Experimental data taken from Holleman-Wiberg as well as from Zhang and coworkers with their suggestions set in bold.^{22,28} Calculated data is given for various functionals (DFAs), simulation temperatures T_{sim} , as well as with and without λ -scaling. All calculations are conducted in the scalar-relativistic (SR) limit except for Ba and Hg, for which (also) spin-orbit (SO) relativistic results are presented.

DFA, T_{sim} , n , κ	$\lambda(E_{\text{coh}}^{\text{DFT}})$	NBP /K	
		direct	λ -scaled
Sodium , $E_{\text{coh}}^{\text{exp}} = -1.113$		lit. 1153– 1163 K	
PBEsol, 1000, 7, 0.60	0.958	1184	1135
PBEsol, 400, 7, 0.70	0.958	1043	1000
Aluminum , $E_{\text{coh}}^{\text{exp}} = -3.390$		lit. 2743 –2793 K	
PBE, 2800, 7, 0.60	0.994	2783	2766
Calcium , $E_{\text{coh}}^{\text{exp}} = -1.840$		lit. 1757– 1760 K	
PBE, 1800, 7, 0.60	0.961	1854	1781
PBE-D3, 1800, 6, 0.60	0.855	2050	1753
PBEsol, 1800, 8, 0.60	0.871	2037	1774
Strontium , $E_{\text{coh}}^{\text{exp}} = -1.720$		lit. 1653 –1657 K	
PBE, 1570, 7, 0.50	1.071	1586	1698
PBE-D3, 1800, 7, 0.60	0.951	1775	1688
PBEsol, 1800, 7, 0.60	0.952	1781	1697
Barium , $E_{\text{coh}}^{\text{exp}} = -1.720$		lit. 1810, ²⁸ 1910 –2173 K	
SR-PBE, 2000, 7, 0.60	1.013	1963	1988
SO-PBE, 2000, 7, 0.60	1.010	1967	1986
PBE-D3, 2000, 7, 0.60	0.915	2144	1961
Manganese , $E_{\text{coh}}^{\text{exp}} = -2.920$		lit. 2235– 2373 K	
PBE, 3200, 7, 0.60	0.751	2924	2197
RPBE, 2400, 8, 0.60	0.916	2309	2115
SCAN, 2400, 8, 0.60	0.980	2082	2041
Copper , $E_{\text{coh}}^{\text{exp}} = -3.490$		lit. 2833– 2868 K	
PBE, 2700, 7, 0.60	1.002	2836	2841
PBE, 3000, 7, 0.60	1.002	2851	2857
Mercury , $E_{\text{coh}}^{\text{exp}} = -0.670$		lit. 629.7– 630.2 K	
SO-PBEsol, 700, 8, 0.60	1.076	591.8	637.0
SR-PBEsol, 700, 8, 0.60	1.227	521.7	640.0

prediction of their neural network of 1600 K. However, they have not considered ref. 28 in their study,²² which provides a value much closer to their estimate. Based on the accurate prediction of the NBPs of Ca and Sr with a very systematic over-estimation of just 2–3%, we conclude that our approach is as accurate for Ba, for which it affords an NBP 1961–1988 K. Correcting for the systematic deviation observed for Ca and Sr yields a value of ≈ 1920 K, which is in excellent agreement with refs. 23,24 and 25, strongly suggesting this value to be correct.

For the heavy metal Hg an accurate account of relativistic effects is essential for accurate properties. Here, the incremental nature of the approach not only enables the inclusion of computationally very demanding spin-orbit coupling (SOC), but also an in-depth analysis of their influence on the physicochemical properties, which we will demonstrate in the following.

The gas phase of Hg consists of weakly interacting atoms with $\Theta = 1$. Spin-orbit relativistic (SO) PBEsol provides a cohesive energy of -0.622 eV (rhombohedral phase) in reasonable agreement with the experiment, yielding a λ of 1.076 (for a detailed discus-

sion of the experimentally lowest structure, see ref. 49). In the scalar-relativistic approximation, *i.e.*, without explicitly accounting for SOC in the valence space, the calculated cohesive energy is distinctly smaller with -0.546 eV resulting in a λ of 1.227. The SO-relativistic calculation provides a NBP of 636.9 K in excellent agreement with the experimental value of 630.2 K. Conducting all calculations in the SR approximation and including SOC only *via* λ -scaling leads to a NBP of 640.1 K (521.7 K before scaling), and thus an only slightly larger deviation from the experiment. This shows that SOC maybe included *via* λ -scaling without losing much accuracy. Note that SOC also has a significant impact on the volume, leading to a significant increase of the density from 11.6 g/ccm (SR) to 12.3 g/ccm (SO). However, as already observed for K, the influence onto the calculated NBP is negligible with 0.1 K.

3.3 Liquid Entropies

In addition to calculating and comparing NBPs, the calculated liquid entropies may be compared directly to experimental ones.³⁹ For this, we obtain experimental entropies by linear interpolation between the four closest values provided in ref. 39 at the corrected effective temperature ($T_{\text{cor}} = \lambda T_{\text{sim}}$), and plot them against the calculated entropies in Fig. 3. Concerning the calculated values, we include the purely classical entropy S used for the linear extrapolation, as well as the sum of classical and electronic entropy $S + S_{\text{el}}$. Inspection of Fig. 3 reveals a picture very consistent with that of the NBPs. In cases where the calculated NBP agrees well with the experimental data, also the entropies are in good agreement, which is perhaps most evident from the example of Mn. It is the element with the largest deviation of the calculated NBP between DFAs, which is reflected in the entropies. Similar to the NBP, SCAN shows a substantial deviation, while PBE agrees reasonably well. The other example with a notable deviation is Ba, and illustrates the disadvantage of a comparison to “experimental” entropies. The problem the entropy is not directly accessible experimentally, but modeled to reproduce various experimental data under certain assumptions, which may be flawed. The only source for the liquid entropy of Ba uses an NBP of 2119 K,³⁹ which is – as previously discussed – most certainly too high. This presumably explains why the deviation of the calculated entropies is more significant for Ba than for Ca and Sr. For all other elements for which experimental data is available (all except Xe), the agreement between calculated and experimental entropies is excellent. Statistical analysis of the shown data (one calculation per element, using PBE-D3 for Ca, Sr and Ba, PBEsol for K, and PBE for Mn) confirms that including the electronic entropy systematically improves the agreement with the experimental data for both temperatures. For the experimental value at the effective temperature, including S_{el} reduces the MD from -5.7 J/(K* mol) (-4.7%) to 1.1 J/(K* mol) (0.7%) and the MAD from 5.8 J/(K* mol) (4.9%) to 2.3 J/(K* mol) (2.0%). In conclusion, this comparison shows that the approach can also provide very accurate liquid entropies with MD below 1%, and moreover, that their accuracy strongly correlates with that of the predicted NBPs.

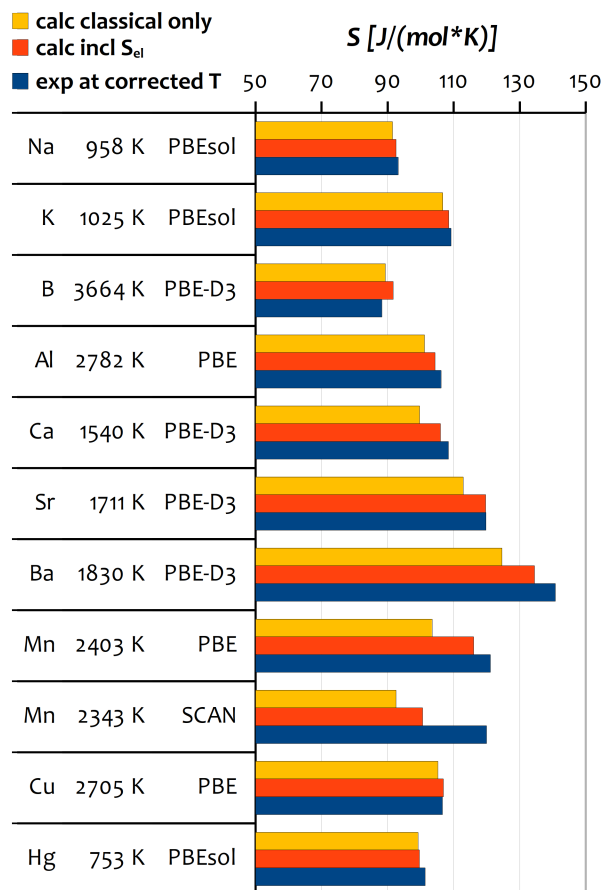


Fig. 3 Calculated liquid entropies excluding (yellow) and including (orange) the electronic entropy compared to experimental values for the corrected temperature (λT_{sim} , given on the x-axis, blue). All values given in J/(mol*K). Experimental values are obtained by linear interpolation between the four closest values from ref. 39.

4 Summary and Conclusion

We have presented and evaluated an approach for the prediction of normal boiling points (NBPs) and entropies of atomic liquids from first principles. The approach efficiently combines thermodynamic integration (TDI) from a non-interacting reference with thermodynamic perturbation theory (TPT) based on plane-wave DFT to provide numerically converged liquid free energies at reasonable computational cost. The incremental scheme not only allows the consideration of computationally demanding effects, like explicit spin-orbit coupling as demonstrated for Hg, but can moreover reveal the impact of each contributions on the NBP as well as other physicochemical properties. Such an analysis revealed that the electronic degeneracy and low-lying excited states of the atoms in the gas phase significantly affect the calculated NBPs, whereas contributions from two-body interactions — direct as well as indirect *via* dimer formation — are negligible for the studied elements.

Calculating the NBPs of a representative set of elements including insulators (Xe), semiconductors (B), alkaline (Na, K), alkaline-earth (Ca, Sr, Ba), transition (Cu, Mn, Hg) and main-group metals (Al), we demonstrated the approach to be robust

with respect to the choice of the density-functional approximation (DFA), and very accurate with an MAD < 2.0%. The only significant deviation between tested DFAs was observed for Mn, which we traced back to the challenging electronic structure of the atom. For B and Ba, the variation between the literature values of the NBP is several times larger (9% and 17%) than the overall MAD of the calculated values. Most notably is Ba, where the deviation of the calculated NBPs is moreover very systematic for the lighter congeners. Accounting for this, our estimate of 1920 K is in excellent agreement with the literature value of 1910 K,^{22–25} questioning the accuracy of other values of 1810 K and well above 2000 K reported elsewhere.^{26–28}

The robustness of the calculated NBPs regarding the choice of the DFA is a result of λ -scaling. The fact that this works so well for the NBP of the studied elements can be rationalized by considering that for their liquid (and solid) to gas transitions, all interatomic forces have to be overcome. As a result, fine details of the potential shape (width, asymptotic behavior etc.) exert only a small influence, whereas the potential depth is crucial. Since λ scaling is based on the relation of the cohesive energies, it very efficiently corrects for the potential depth. As a result, any λ -scaled method or DFA that affords a reasonable liquid structure (and a good account of the electronic entropy) can provide accurate NBPs. Interestingly, as we have learned from other ongoing projects, an entirely different picture emerges for the melting point, which does strongly depend on the shape and particularly the width of the potential.¹⁶ This will be explored in more detail in forthcoming projects.

Besides the NBPs, also calculated liquid entropies were shown to be in excellent agreement with reference values,³⁹ while their accuracy correlated with that of the NBPs. The mean deviation (MD) from the references over all examples is just 2.0% or 1.1 J/(mol*K). Since the calculation of the NBPs requires the free-energy of the gas phase, whose calculation becomes tedious if several low-lying electronic states and/or molecular species are present, this direct comparison of entropies expands the scope of systems for which the approach can be tested.

One limitation of the presented approach in its current form is that it is only applicable to structurally simple systems that constitute a global minimum on the potential-energy surface, which essentially excludes molecular systems. The underlying problem is that a presence of complex structure conflicts with the reversibility-criterion of the TDI, since covalent bonds are readily broken and reformed at low interacting strength. We are currently testing a modification of this approach which overcomes this limitation.

5 Computational Details

All DFT calculations have been carried out with VASP 5.4.4.^{50–53} The core region is modeled using the projector-augmented wave (PAW) approach of Joubert and Kresse using the softest potential available in the VASP library.^{54,55} For Cn and Og, the PAW potentials and D3 parameters introduced in ref. 56 were used. Calculations with the SCAN functional take into account non-spherical contributions from the PAW potentials (LASPH = TRUE) through TPT. The volume calculations were conducted in the

Γ -point approximation, or, if there was a significant non-linear influence, with a 2^3k -point grid (B, Al and Cu). Thermodynamic integration was conducted with the lower energy cut-off shown in Tab. 6 in the Γ -point approximation, except for B and Hg, where a 2^3 grid was employed. Thermostatting was done with a Nosé-Hoover thermostat with SMASS = 2–4, SCF convergence (ECONV) reduced to 10^{-4} , and PREC = normal. The timestep was chosen for each case based on atomic mass and simulation temperature, and further reduced if necessary to ensure accurate thermostatting. For the integration point closest to the non-interacting limit, the timestep is reduced significantly to stabilize the simulation numerically. In few cases with particularly small λ values, it was required to switch to a Langevin thermostat with a very large friction coefficient (LANGEVIN_GAMMA = 8+). In general, each integration point was sampled with at least about 10000 steps, of which the first 2000 are considered equilibration. The length of each simulation was chosen such that the statistical error of the NBP is below 0.2%. For thermodynamic perturbation theory, several single-point calculations are conducted for 10–20 statistically independent snapshots taken from the trajectory with $\lambda = 1$; one with the same settings as the simulation, one with the increased cut-off, precision and convergence criteria (PREC = accurate, ECONV = 10^{-6}), and finally one with all settings from above as well as a finer k -point grid as specified in Tab. 6. The contributions from these steps are shown for Xe, K and B in Tab. 1.

Conflicts of interest

There are no conflicts to declare.

Acknowledgements

JMM acknowledges financial support by the Alexander-von-Humboldt Foundation (Bonn) and the use of New Zealand eScience Infrastructure (NeSI) high performance computing facilities (nesi000474). The author wants to thank O. Smits, A. Hansen, S. Grimme and S. Schmitz for helpful comments on the manuscript.

Notes and references

- 1 H. Gomez, M. Bures and A. Moure, *Philosophical Transactions of the Royal Society A: Mathematical, Physical and Engineering Sciences*, 2019, **377**, 20180203.
- 2 O. Sugino and R. Car, *Phys. Rev. Lett.*, 1995, **74**, 1823–1826.
- 3 A. D., M. J. Gillan and G. D. Price, *The Journal of Chemical Physics*, 2002, **116**, 6170–6177.
- 4 D. Alfè, L. Vočadlo, G. D. Price and M. J. M. J. Gillan, *J. Phys. Condens. Matter*, 2004, **16**, S973—S982.
- 5 B. Grabowski, L. Ismer, T. Hickel and J. Neugebauer, *Phys. Rev. B*, 2009, **79**, 134106.
- 6 L.-F. Zhu, B. Grabowski and J. Neugebauer, *Phys. Rev. B*, 2017, **96**, 224202.
- 7 U. R. Pedersen, F. Hummel, G. Kresse, G. Kahl and C. Dellago, *Phys. Rev. B*, 2013, **88**, 094101.
- 8 H. Nakai and A. Ishikawa, *The Journal of Chemical Physics*, 2014, **141**, 174106.

- 9 A. V. Marenich, C. J. Cramer and D. G. Truhlar, *The Journal of Physical Chemistry B*, 2009, **113**, 6378–6396.
- 10 S. Hilal, S. Karickhoff and L. Carreira, *QSAR & Combinatorial Science*, 2003, **22**, 565–574.
- 11 P. Y. Chan, C. M. Tong and M. C. Durrant, *Journal of Molecular Graphics and Modelling*, 2011, **30**, 120 – 128.
- 12 M. R. Fissa, Y. Lahiouel, L. Khaouane and S. Hanini, *Journal of Molecular Graphics and Modelling*, 2019, **87**, 109 – 120.
- 13 K. JOBACK and R. REID, *Chemical Engineering Communications*, 1987, **57**, 233–243.
- 14 S. Alavi and D. L. Thompson, *Molecular Simulation*, 2006, **32**, 999–1015.
- 15 N. Gaston, *Advances in Physics: X*, 2018, **3**, 1401487.
- 16 J.-M. Mewes, O. R. Smits, G. Kresse and P. Schwerdtfeger, *Angewandte Chemie International Edition*, 2019, **58**, 17964–17968.
- 17 D. M. Eike and E. J. Maginn, *The Journal of Chemical Physics*, 2006, **124**, 164503.
- 18 Y. Zhang and E. J. Maginn, *The Journal of Chemical Physics*, 2012, **136**, 144116.
- 19 F. Dorner, Z. Sukurma, C. Dellago and G. Kresse, *Phys. Rev. Lett.*, 2018, **121**, 195701.
- 20 M. Rang and G. Kresse, *submitted*, 2019.
- 21 K. S. Pitzer, *J. Chem. Phys.*, 1975, **63**, 1032–1033.
- 22 Y. Zhang, J. R. G. Evans and S. Yang, *Journal of Chemical & Engineering Data*, 2011, **56**, 328–337.
- 23 J. G. Stark and H. G. Wallace, *Chemistry Data Book*, John Murray: London, 1982, reprint 1984, pp. 8–11, 50–51.
- 24 J. G. Speight, N. A. Lange and J. A. Dean, *Lange's Handbook of Chemistry*, 16th ed., McGraw-Hill: New-York, 2005, pp. 1.18–1.62, 1.124–1.127, 1.280–1.298.
- 25 J. Emsley, *The Elements*, 3rd ed., Clarendon Press: Oxford, 1998, pp. 1.18–1.62, 1.124–1.127, 1.280–1.298.
- 26 G. W. Kaye and T. H. Laby, *Tables of Physical and Chemical Constants*, 16th ed., Longman: Harlow, 1995, pp. 212–214, 338–342.
- 27 W. M. Haynes, D. R. Lide and T. J. Bruno, *CRC Handbook of Chemistry and Physics: A Ready-reference Book of Chemical and Physical Data*, 97th ed., CRC Press: Boca Raton, FL, 2016–2017, pp. 4–49.
- 28 A. F. Holleman and N. Wiberg, *Lehrbuch der Anorganischen Chemie*, de Gruyter, Berlin; New-York, 101st edn, 1995.
- 29 N. D. Mermin, *Phys. Rev.*, 1965, **137**, A1441–A1443.
- 30 J.-M. Mewes, P. Jerabek, O. R. Smits and P. Schwerdtfeger, *Angewandte International Edition*, just accepted, 2019.
- 31 O. R. Smits, P. Jerabek, E. Pahl and P. Schwerdtfeger, *Phys. Rev. B*, 2020, **101**, 104103.
- 32 J. P. Perdew, K. Burke and M. Ernzerhof, *Phys. Rev. Lett.*, 1996, **77**, 3865–3868.
- 33 J. P. Perdew, K. Burke and M. Ernzerhof, *Phys. Rev. Lett.*, 1997, **78**, 1396.
- 34 Y. Zhang and W. Yang, *Phys. Rev. Lett.*, 1998, **80**, 890–890.
- 35 S. Grimme, J. Antony, S. Ehrlich and H. Krieg, *J. Chem. Phys.*, 2010, **132**, 154104.
- 36 S. Grimme, S. Ehrlich and L. Goerigk, *Journal of Computational Chemistry*, 2011, **32**, 1456–1465.
- 37 P. Jerabek, O. Smits, E. Pahl and P. Schwerdtfeger, *Mol. Phys.*, 2018, **116**, 1–8.
- 38 L. Schimka, R. Gaudoin, J. c. v. Klimeš, M. Marsman and G. Kresse, *Phys. Rev. B*, 2013, **87**, 214102.
- 39 Malcom W. Chase, Jr., *J. Phys. Chem. Ref. Data, Monograph No. 9*, 1998.
- 40 M. Griffel, *The Journal of Chemical Physics*, 1953, **21**, 1908–1908.
- 41 F. Weinhold, *The Journal of Chemical Physics*, 1998, **109**, 367–372.
- 42 M. von Domaros, E. Perlt, J. Ingenmey, G. Marchelli and B. Kirchner, *SoftwareX*, 2018, **7**, 356 – 359.
- 43 B. Cowan, *Topics in Statistical Mechanics*, Imperial College Press, 2005, vol. 3.
- 44 E. Caldeweyher, J.-M. Mewes, S. Ehlert and S. Grimme, *Phys. Chem. Chem. Phys.*, 2020, –.
- 45 M. J. van Setten, M. A. Uijtewaal, G. A. de Wijs and R. A. de Groot, *Journal of the American Chemical Society*, 2007, **129**, 2458–2465.
- 46 K. K. Verma, J. T. Bahns, A. R. Rajaei-Rizi, W. C. Stwalley and W. T. Zemke, *The Journal of Chemical Physics*, 1983, **78**, 3599–3613.
- 47 V. O. Kiohara, E. F. Carvalho, C. W. Paschoal, F. B. Machado and O. Roberto-Neto, *Chemical Physics Letters*, 2013, **568–569**, 42 – 48.
- 48 J. R. Lombardi and B. Davis, *Chemical Reviews*, 2002, **102**, 2431–2460.
- 49 K. G. Steenbergen, J.-M. Mewes, L. F. Pasteka, H. W. Gaggeler, G. Kresse, E. Pahl and P. Schwerdtfeger, *Phys. Chem. Chem. Phys.*, 2017, **19**, 32286–32295.
- 50 G. Kresse and J. Hafner, *Phys. Rev. B*, 1993, **47**, 558.
- 51 G. Kresse and J. Hafner, *Phys. Rev. B*, 1994, **49**, 14251.
- 52 G. Kresse and J. Furthmüller, *Phys. Rev. B*, 1996, **54**, 11169.
- 53 G. Kresse and J. Furthmüller, *Comp. Math. Sci.*, 1996, **6**, 15.
- 54 P. E. Blöchl, *Phys. Rev. B*, 1994, **50**, 17953.
- 55 G. Kresse and D. Joubert, *Phys. Rev. B*, 1999, **59**, 1758.
- 56 L. Trombach, S. Ehlert, S. Grimme, P. Schwerdtfeger and J.-M. Mewes, *Phys. Chem. Chem. Phys.*, 2019, –.

6 Supporting Information

In addition to the information presented on the following pages, we provide the spreadsheets (in open-document format) used to conduct all calculations starting from the raw data (simulation averages) to the final boiling points.

6.1 Calculation of the Liquid Free Energy

The free energy of the liquid is calculated through TDI from a non-interacting reference (ideal gas). For this purpose the difference of the internal energies is integrated along the a coupling parameter λ

$$\Delta G_{0-1} = \int_0^1 d\lambda \langle U_1(\mathbf{R}) - U_0(\mathbf{R}) \rangle_\lambda, \quad (3)$$

which relates the liquid with U_1 to the ideal gas with U_0 at the same T and V by scaling the forces, and added to the free energy of the ideal gas (eqs. 7 and 8). This integral is evaluated using numerical quadrature in the form of a n -point Gauss-Lobatto rule, in principle requiring one NVT simulation for each λ . Although most of these simulations are straightforward, the ones very close to the ideal-gas limit ($\lambda \ll 0.01$ or $< 1\%$ of the DFT forces) are tedious, whereas and the simulation for the end point $\lambda = 0$ is hardly possible with a PAW+DFT methodology. This is because close-encounters between the (almost) non-interacting atoms lead to singularity in the energy resulting in numerical instabilities in errors in the simulations, partly resulting from overlapping core-electrons. An approach to circumvent these issues was devised and implemented by Kresse and coworkers and will be used here with slight modifications.¹⁹

The approach is based on substituting λ in eq. (3) with $\lambda(x) = \frac{x+1}{2}^{1/(1-k)}$, which yields

$$\Delta G = \frac{1}{2(1-\kappa)} \int_{-1}^1 f(\lambda(x)) \lambda(x)^\kappa dx. \quad (4)$$

Note that this introduces an explicit dependency on λ in the integrand, which not only dampens the impact of the technically challenging calculations near the non-interacting limit (*cf.* effective weights in Fig. 4), but also completely eliminates the point for $\lambda = 0$. The substitution also introduces a parameter κ to influence the mapping of the quadrature points between the domains. While a value close to 0 retains the original (equidistant) spacing of the Gauss-Lobatto quadrature, choosing κ close to 1 increases the density of quadrature points in the λ domain in the region close to $\lambda = 0$, where the slope of $f(\lambda)$ is the largest (*cf.* Fig. 4). While Kresse and coworkers suggest $\kappa > 0.8$, we demonstrated here that at least for the calculation of NBPs, much smaller values suffice. This dramatically reduces the computational effort as it allows to avoid the technically challenging simulations near the non-interacting limit almost entirely.

Since it is nevertheless prohibitively expensive to carry out the TDI at a converged level of theory, it is instead combined with thermodynamic perturbation theory (TPT)

$$\Delta G_{1-2} = -\frac{1}{\beta} \ln \langle e^{-\beta[U_2(\mathbf{R}) - U_1(\mathbf{R})]} \rangle_1, \quad (5)$$

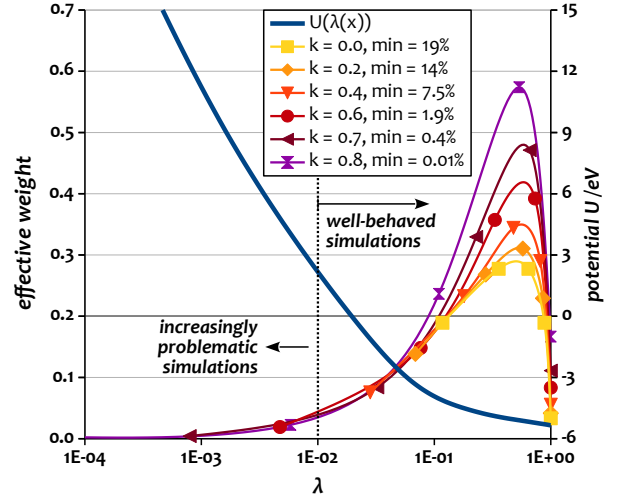


Fig. 4 Effective weight plotted against the λ s (logarithmic scale) at which simulations have to be conducted for a 6-point Gauss-Lobatto rule for several different choices of κ . The interaction-strength the most “non-interacting” simulation (min) is given in the legend in %. For reference, the evolution of the value of the integrand taken from B at 4000 K with PBE-D3 is shown in blue on the secondary axis. The effective weight is $(w_i \lambda^\kappa) / (2(1-\kappa))$ where w_i is the weight from the respective Gauss-Lobatto rule.

where the index after the angle bracket indicates that the difference ΔU_{1-2} is evaluated for configurations generated by H_1 . Thus, by exploiting the linear shift of a refined Hamiltonian (*e.g.* increased cut-off, k -points or even another functional), TPT can often provide a very good estimate for the respective free-energy difference from as few as 5-20 single-point calculations. Instead of the exact equation, we use the second-order cumulant expansion

$$\Delta G_{1-2} \approx \langle \Delta U \rangle_1 - \frac{\beta}{2} \langle (\Delta U - \langle \Delta U \rangle)^2 \rangle_1, \quad (6)$$

which is sufficiently accurate since already the second-order term is $\ll 1$ meV/atom in all cases, and can thus be neglected. Using TPT, all final results are converged to within ≈ 2 meV/atom, which translates into a error in the NBP of about 2 K.

6.2 Calculation of the Gaseous Free Energy

The free energy of the gas phase is calculated for the non-interacting (ideal) gas at its equilibrium volume. For a given atomic degeneracy Θ , volume V , temperature T , particle number N and mass m this is

$$G^{\text{id}} = -\frac{1}{\beta} \ln(Z(T, V, N)), \quad \text{with} \quad (7)$$

$$Z(T, V, N) = \frac{(\Theta V)^N}{\Lambda^{3N} N!} \quad \text{and} \quad \Lambda = h \sqrt{\frac{\beta}{2\pi m}}. \quad (8)$$

For the gas phase, this equation is solved using the Stirling approximation, which is sufficiently accurate since we are considering an arbitrary number of particles. The same equation is also used to calculate the free energy of the non-interacting reference for the liquid (at the equilibrium volume of the liquid). Here, however, the Stirling approximation is no longer suitable since

the number of particles is finite (61 or 64). Moreover, since – in contrast to the real atoms in the gas phase – the non-interacting reference for the liquid consists of hypothetical point-masses, they are not degenerate.

To validate the accuracy of the non-interacting model, we evaluate the first virial (two-body) correction for each of the examples assuming a Lennard-Jones (12,6) potential with the parameters derived from first-principles calculations for the respective dimers. This leads to the following integral

$$G_{\text{LJ}}^g = G_{\text{id}}^g - \frac{2\pi N^2}{V\beta} \int \left[r^2 e^{-4\epsilon\beta \left[\left(\frac{\sigma}{r}\right)^{12} - \left(\frac{\sigma}{r}\right)^6 \right]} - 1 \right] dr \quad (9)$$

which can be evaluated as described in ref. 43. This provides generally very small corrections (≤ 1.0 meV/atom), which in turn have a negligible impact on the calculated boiling points (≤ 1 K).

7 Determination of Equilibrium Volumes

To calculate the equilibrium volume, the 61 or 64-atom supercells are simulated with the default settings (*cf.* Tab. 6) at several slightly different volumes until the statistical average of the pressure is converged to within 0.3 kBar. For about 5-20 equidistant snapshots from the trajectory, single-point calculations are conducted with the converged settings to obtain a correction for the influence of Pulay stress, a finer k -point grid, and increased numerical precision (as well as spin-orbit coupling in case of Ba, Hg, Cn and Og). The corrected pressures at each point are fitted with a second-order polynomial and interpolated to the x -intersection ($p = 0$). Final volumes are confirmed during the TDI, where the simulation with $\lambda = 1$ and subsequent TPT provides the residual pressures given in Tab. 4, along with the calculated atomic volumes and corresponding densities.

Table 4 Calculated equilibrium volumes (in $\text{\AA}^3/\text{atom}$), corresponding densities ρ (in g/cm^3), and residual pressures (in kBar) for all studied elements. Volumes of Al, Cu, B, and Cn are calculated with 2^3k -point grid in the simulations, all others employ the Γ -point approximation and include the effect of more k -points perturbatively.

element/DFA/ T_{sim}	V/atom	ρ	residual p
Xe/PBE-D3/165 K	79.8	2.73	0.1
Xe/PBE-D3/200 K	85.8	2.54	0.1
Xe/revPBE-D3/165 K	79.8	2.73	-0.1
K/PBE/1000 K	90.42	0.718	0.0
K/PBEsol/1000 K	93.22	0.696	0.3
K/PBE-D3/1000 K	101.9	0.637	0.1
B/PBE-D3/4000 K	8.820	2.04	-0.2
Al/PBE/2800 K	23.62	1.90	0.1
Na/PBEsol/1000 K	46.24	0.825	0.2
Ca/PBE/1800 K	52.51	1.27	-0.5
Ca/PBED3/1800 K	47.63	1.40	0.2
Ca/PBEsol/1800 K	49.22	1.35	-0.2
Sr/PBE/1570 K	66.92	2.17	0.0
Sr/PBED3/1800 K	64.00	2.27	-0.2
Sr/PBEsol/1800 K	65.55	2.22	-0.7
Ba/PBE/2000 K	81.25	2.81	0.0
Ba/PBED3/2000 K	73.40	3.11	0.1
Mn/PBE/3200 K	12.75	7.16	0.5
Mn/RPBE/2400 K	12.49	7.30	-0.4
Mn/SCAN/2400 K	11.58	7.89	-1.2
Cu/PBE/2400 K	12.49	7.30	-0.4
Hg/SO-PBEsol/700 K	25.86	12.9	-0.1

Table 5 Calculated free energies, internal energies (in eV/atom), as well as classical and electronic entropies (in meV/[atom*K]) for the liquid phase of all studied elements.

DFA, T_{sim} , T_{eff}	G	U	S	S_{el}
Xenon				
PBE-D3, 165, 165	-0.2368	-0.1406	0.5831	0.0
Sodium				
PBEsol, 1000, 959	-1.8091	-0.8605	0.9486	0.0112
Potassium				
PBE, 1000, 1073	-1.6822	-0.5685	1.1137	0.0200
PBE-D3, 1000, 945	-1.7617	-0.6803	1.0822	0.0182
PBEsol, 1000, 1002	-1.7311	-0.6371	1.0940	0.0188
Boron				
PBE-D3, 4000, 3664	-8.5304	-4.8373	0.9233	0.0248
Aluminum				
PBE, 2800, 2782	-5.5099	-2.5913	1.0488	0.0327
Calcium				
PBE, 1800, 1729	-3.2486	-1.3322	1.0644	0.0658
PBE-D3, 1800, 1540	-3.4238	-1.5414	1.0327	0.0657
PBEsol, 1800, 1568	-3.4256	-1.5298	1.0458	0.0656
PBEsol, 2100, 1829	-3.7680	-1.4770	1.0909	0.0755
Strontium				
PBE, 1570, 1680	-2.9156	-1.1088	1.1509	0.0621
PBE-D3, 1800, 1712	-3.3560	-1.2506	1.1697	0.0707
PBEsol, 1800, 1714	-3.3618	-1.2305	1.1841	0.0708
Barium				
PBE, 2000, 2026	-3.9186	-1.2899	1.3144	0.1088
PBE-D3, 2000, 1830	-4.0781	-1.4942	1.2920	0.1020
Manganese				
PBE, 3200, 2402	-6.3447	-2.9140	1.0721	0.1307
RPBE, 2400, 2198	-4.7648	-2.3975	0.9852	0.0987
SCAN, 2400, 2342	-4.4795	-2.1522	0.9697	0.0833
Copper				
PBE, 2700, 2705	-5.5273	-2.5896	1.0881	0.0175
PBE, 3000, 3006	-5.8769	-2.5039	1.1243	0.0220
Mercury				
SO-PBEsol, 700, 753	-1.0814	-0.3609	1.0279	0.0045

Table 6 Settings used for the DFT-MD calculations in the thermodynamic integration and perturbation theory. The reduced timestep used in the simulations near the non-interaction limit is given in parenthesis.

element	cut-off	k -grid	timestep [fs]
Xe (165 K, 200 K)	200 \rightarrow 400	$\Gamma \rightarrow 2^3$	8 (4)
K (923 K, 1023 K, 1123 K)	200 \rightarrow 400	$\Gamma \rightarrow 3^3$	8 (1)
K (1000 K)	250 \rightarrow 500	$\Gamma \rightarrow 2^3$	4 (1)
Na (1000 K)	250 \rightarrow 500	$\Gamma \rightarrow 2^3$	4 (1)
B (4000 K)	350 \rightarrow 600	$2^3 \rightarrow 3^3$	1 (0.25)
Al (2800 K)	400 \rightarrow 600	$\Gamma \rightarrow 2^3$	2 (1)
Ca (1800 K, 2100 K)	200 \rightarrow 400	$\Gamma \rightarrow 2^3$	4 (1)
Sr (1800 K)	200 \rightarrow 400	$\Gamma \rightarrow 2^3$	4 (1, 0.5)
Ba (2000 K)	200 \rightarrow 400	$\Gamma \rightarrow 2^3$	5 (0.5)
Cu (2700 K, 3000 K)	350 \rightarrow 600	$\Gamma \rightarrow 2^3$	2 (1)
Mn (2400 K)	300 \rightarrow 600	$\Gamma \rightarrow 2^3$	2 (1)
Mn (3200 K)	300 \rightarrow 600	$\Gamma \rightarrow 2^3$	1.5 (0.3)
SR/SO Hg (700 K)	250 \rightarrow 500	$2^3 \rightarrow 3^3$	12 (3)